

Study on the solar albedo characteristics of pavement and embankment slope surfaces in permafrost regions

Ruiqiang Bai ^{a,b}, Mingyi Zhang ^{a,b,*}, Jiwei Wang ^c, Guanji Li ^{a,b}, Zhilang You ^{a,b}

^a State Key Laboratory of Frozen Soil Engineering, Northwest Institute of Eco-Environment and Resources, Chinese Academy of Sciences, Lanzhou 730000, China

^b University of Chinese Academy of Sciences, Beijing 100049, China

^c Institute of Transportation, Inner Mongolia University, Hohhot 010070, China



ARTICLE INFO

Keywords:

Solar albedo
Permafrost regions
Measurement method
Thermal stability
Embankment surface
Slope surface

ABSTRACT

Roadways built in permafrost regions are more sensitive to the thermal disturbance caused by the natural environment and engineering construction activities. The construction of the embankment changes the albedo characteristics of the natural ground surfaces. Dark asphalt pavement absorbs a huge amount of solar radiation into the permafrost embankment, which leads to the thawing of frozen soil and freezing-thawing diseases of the embankment. Besides, the south-facing slope of the high-fill embankment is exposed to longer and stronger insolation than the north-facing slope annually. It gives rise to the thermal asymmetrical problem and differential settlement across the embankment. To solve above problems and further improve the thermal stability of permafrost embankment, we study the solar albedo characteristics of pavement and embankment slope surfaces in permafrost regions. In this study, an albedo measurement method is proposed for both pavement surface and slope surfaces. The method is validated by in-situ experiments and compared with traditional albedo measurement methods. Meanwhile, we measure the albedo values of the permafrost embankment surfaces along the G109 Highway in high latitude permafrost regions by using the proposed method. The results show that these embankment surfaces absorb a lot of solar radiation for a long time due to the low albedo. Comparing the measured results and remote sensing data, we carry out a comprehensive analysis of the albedo characteristics of permafrost embankment surfaces. Based on these findings, a preliminary solution is put forward to improve the thermal stability of permafrost embankment and decrease embankment diseases.

1. Introduction

It is always challenging to build roads in permafrost regions because the frozen soils in the roadbed could melt due to the thermal disturbance caused by the engineering constructions and special climatic conditions (Jin et al., 2008). To decrease the influence of thermal disturbance on the embankment stability and service performance, a series of innovative embankment designs have been developed, including thick embankments (Cheng et al., 2008), crushed-rock embankments (Pei et al., 2017a), duct-ventilated embankments (Zhang et al., 2021), insulation board embankments (Cai et al., 2016), thermosyphon-inserted embankments (Pei et al., 2017b), and the combination of these embankments (Lai et al., 2009; Pei et al., 2021). These designs reduce the internal temperature of the roadbed as a result of convective heat transfer or heat rejection techniques, which shows good cooling

performance. However, these techniques do not reduce the absorption of solar radiation by the embankment from the source (Zhang et al., 2018). With the development of highways and expressways, the embankment will be built wider, and the dark asphalt concrete materials will be used extensively on pavement surfaces. High-grade asphalt pavement will absorb a great deal of solar radiation. The large quantities absorbed energy will be stored in the roadbed. These effects reduce the thermal stability of permafrost embankment and cause roadbed diseases. Especially in the high latitude permafrost regions, such problems are more prominent due to more intense solar radiation and longer daylight hours. Reducing the solar absorption of the embankment surface has been proved to be an effective way of improving thermal stability. One way is to cover the pavement or slope surface with shading boards to insulate from solar radiation (Yu et al., 2008). But this kind of strategy is costly and vulnerable to high-speed winds. Another method is coating

* Corresponding author at: State Key Laboratory of Frozen Soil Engineering, Northwest Institute of Eco-Environment and Resources, Chinese Academy of Sciences, Lanzhou 730000, China.

E-mail address: myzhang@lzb.ac.cn (M. Zhang).

the embankment surfaces with high reflectivity pigments (Chou et al., 2012).

In addition to these problems, permafrost embankments also suffer from thermal asymmetrical problems (Liu et al., 2017). In the northern hemisphere, the south-facing side slopes are exposed to greater solar radiation than the north-facing ones. Consequently, the permafrost roadbed under the southern side slope is warmer and more likely to melt than the northern side. The southern road shoulder settles more quickly, which leads to differential settlement across the embankment (Zhang et al., 2017). This phenomenon is commonly known as the sunny-shade slope effect in permafrost regions (Chou et al., 2008). Resulting roadbed diseases have been widely observed in the Qinghai-Tibet Highways (Fig. 1). Enhanced convective heat transfer on the southern slope of the roadbed is an effective solution. Corresponding techniques include the crushed-rock layers and thermosyphons (Tai et al., 2018). Another cost-effective strategy is to adjust the solar albedo of the pavement or embankment slopes on both sides by coating heat-reflective pigments (Doré et al., 2016; Qin et al., 2016a). To achieve this measure, we should clarify the reflectivity characteristics of the embankment surfaces.

Defined as the reflected proportion of incident solar radiation, solar albedo is a key parameter to determine the solar absorption for a specific engineering surface. While researches on the measurement methods of solar albedo for low-slope surfaces are plentiful, the measurement method of embankment slope surfaces remains defective at the present stage (Qin et al., 2018; Qin et al., 2016b). As for a homogeneous flat surface, the surface reflectance can be determined by a solar reflectometer based on ASTM-C1549-09 (ASTM-C1549-09, 2002) or a solar spectrophotometer based on ASTM-E903-12 (ASTM-E903-12, 2012). Fernández-García et al. (Fernández-García et al., 2017) reviewed the equipment and methods for measuring surface reflectance in the laboratory. However, these methods are not appropriate for the in-situ albedo measurement of embankment slope surfaces. The pyranometer measurement method based on ASTM-E1918-06 (ASTM-E1918-06, 2006) is an effective technique to determine the in-field surface albedo. For this method, Levinson et al. (Levinson et al., 2010a, b; Levinson et al., 2020) summarized some common measuring methods of surface reflectance for laboratory tests and engineering applications. The mentioned methods are more suitable for low-slope surfaces, such as flat ground or curved roofing (Akbari et al., 2008). To understand the albedo difference between flat surface and embankment surface, Qin et al. (Qin et al., 2016b) proposed a theory and procedure for measuring the albedo of a road embankment with slope surface through a simplified prototype. The results showed that the albedo of a typical embankment surface is about 0.05 to 0.08 lower than a flat surface made up of the same material. This method can be further studied on a real engineering slope surface on account of some limitations of the prototype model. It is always challenging to determine the engineering slope surface under complex conditions. These traditional methods would lead to measurement errors when the slope angle is higher or the slope length is shorter. If a slope surface is shadowed, the albedo measurement would deviate far from the true value since the upper sensor always receives the total incident radiation, but the lower sensor can't receive the reflected radiation of beam radiation. The albedo measurement methods for a

limited area may be useful to solve the above problems, but these methods are not verified on engineering slope surface in previous researches (Sailor et al., 2006; Qin et al., 2016a; Mei et al., 2017). The main reasons can be summarized as follows. Firstly, there are insufficient publications on the instruments and procedures of albedo measurement for embankment slope surfaces to refer to. Besides, the experimental site is difficult to select because it need to satisfy the relevant testing and experimental conditions, such as open field and abundant solar radiation. Last but not the least, it is hard to obtain accurately incident solar short-wave radiation (hereafter incident radiation) and reflected solar short-wave radiation (hereafter reflected radiation) of slope surface compared with a horizontal surface in consideration of multiple reflectance effects and different slope conditions, such as orientations, angles, positions, albedos, and materials.

Based on the current state of knowledge and shortcomings, we study the solar albedo characteristics of embankment surfaces in high-altitude permafrost regions. First of all, an albedo measurement method is proposed for both pavement surface and slope surfaces. The method is validated by in-situ experiments and compared with other albedo measurement methods. Then, the albedo values of the permafrost embankment surfaces along the G109 Highway are evaluated by the proposed method. Comparing the measured results and remote sensing data, we carry out a comprehensive analysis of the surface albedo characteristics of permafrost embankment. Finally, a preliminary solution to improve the thermal stability of permafrost embankment and decrease the embankment diseases is proposed.

2. Theory and method

2.1. The albedo of a flat homogeneous surface

Albedo is defined as the ratio of solar radiation of all wavelengths reflected by a surface to the amount of incident upon it. As for a homogeneous and flat surface, its albedo or reflectivity can be calculated by:

$$\rho_{\lambda_0 \rightarrow \lambda_1} = \left(\int_{\lambda_0}^{\lambda_1} \rho(\lambda) i(\lambda) d\lambda \right) / \int_{\lambda_0}^{\lambda_1} \rho(\lambda) d\lambda \quad (1)$$

where ρ is the albedo of the test surface for a given wavelength range; i is the incident solar spectral irradiance, $\text{W}/\text{m}^2/\text{nm}$; λ is the wavelength, nm ; $\rho(\lambda)$ is the spectral reflectance; λ_0 and λ_1 are taken as 250 nm and 2800 nm, respectively. Based on Eq. (1), we can determine the albedo of a flat homogeneous surface, including the black shade ring and reference mask used in this study (Fig. 2).

2.2. Theoretical methods in determining the solar albedo of embankment slope surfaces

Different from other engineering slope surfaces, such as roofing surfaces, the measured albedo of the embankment slope surface is also influenced by the solar position and surrounding environment. The reflected radiation signal received by the lower pyranometer is not only influenced by the view factor of the detector to the measured area, but



Fig. 1. Typical diseases of the permafrost embankments along the G109 Highway.

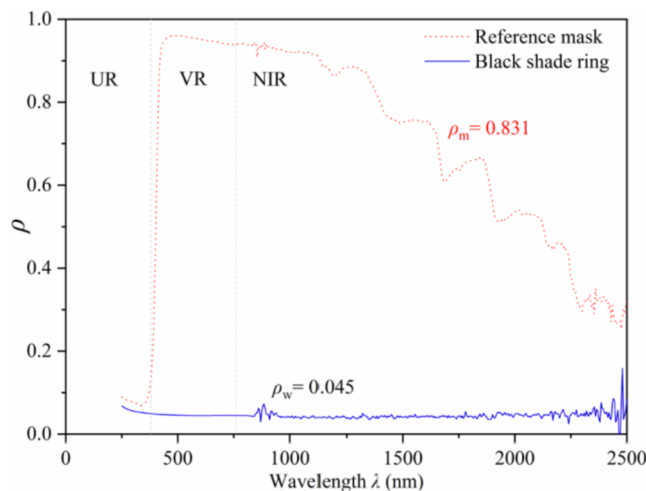


Fig. 2. The spectral reflectance of black shade ring and reference mask.

also affected by the solar position and surrounding environment. The differences are more obviously embodied in the finite slope surface and the shadowed area. The conventional methods for measuring surface albedo may be not applicable in this kind of engineering condition. Therefore, an improved method based on the study of Qin et al. (Qin and He, 2017) was used to measure the slope surface albedo for engineering applications. The measuring system and detailed schematic are shown in Fig. 3 and Fig. 4, respectively. In this study, a black shade ring is used to obtain a limited measurement area on the slope surface. The shade ring can isolate the radiations that are not reflected by the slope surface, such as the solar short-wave radiation and the radiations reflected by the surrounding ground surface (Fig. 4). Meanwhile, the low-reflected inner surfaces of the black shade ring can decrease the multiple reflections, which could influence the measurement results. A calibration device is used to make sure that both upper and lower pyranimeters are parallel to the target area during the measurement.

The height of the black shade ring, h_w , is a key parameter that can be derived as

$$h_w = \frac{r_a + r_d}{r_d} \left(h_d - \frac{r_t h_d}{r_t + r_d} \right) \quad (2)$$

where r_d represents the radius of the pyranometer detector; r_w represents the radius of the shade ring's interior wall; r_a represents the radius of nonopaque aperture; r_t represents the radius of the measured area; h_w denotes the height of shade ring; h_d represents the height of lower detector. It is worth emphasizing that both upper and lower pyranometers are parallel to the slope surface and influenced by the multiple reflection effect from surrounding ground surface. The slope angle η is in the 0–90°

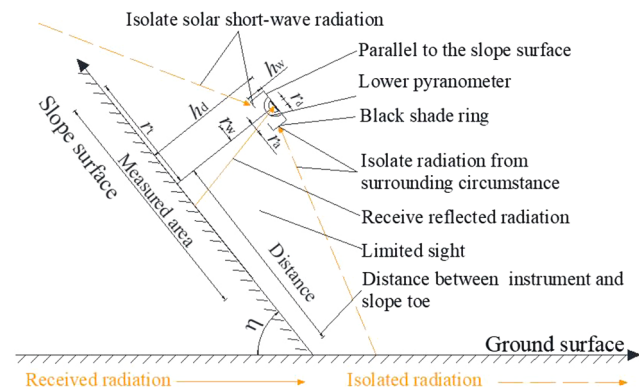


Fig. 4. Detailed schematic of the measurement theories.

range. Detailed schematic and parameters of the black shade ring refer to Fig. 5.

In this configuration, the incident radiation received by the upper pyranometer I_s can be directed read from the logger device. The reflected radiation received by the lower pyranometer includes the reflections from the shaded portion on the target, from the unshaded portion on the target, from the shade ring's interior surface, and from the other part of the shade ring. When the slope surface is uncovered by the reference mask, the reading of the lower pyranometer is

$$R_s = I_s \rho_s F_{d-\text{usd}} + k I_s \rho_s F_{d-\text{sd}} + I_s \rho_s F_{w-\text{sd}} \rho_w F_{d-\text{w}} + I_s \rho_{\text{sur}} F_{w-\text{sur}} \rho_w F_{d-\text{w}} + R_e \quad (3)$$

A reference mask is used to decrease the measurement error and the influence of the shadowed area. When the slope surface is covered by the reference mask, the reading of the lower pyranometer is

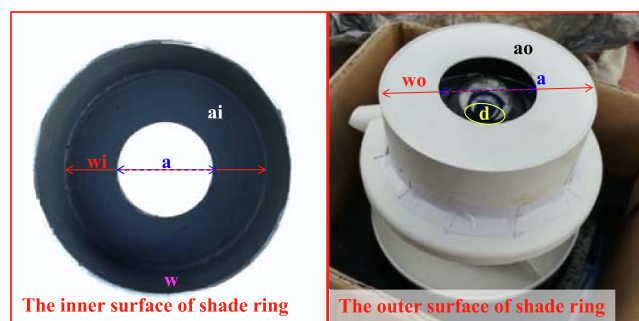


Fig. 5. Schematic and relevant parameters of the black shade ring.

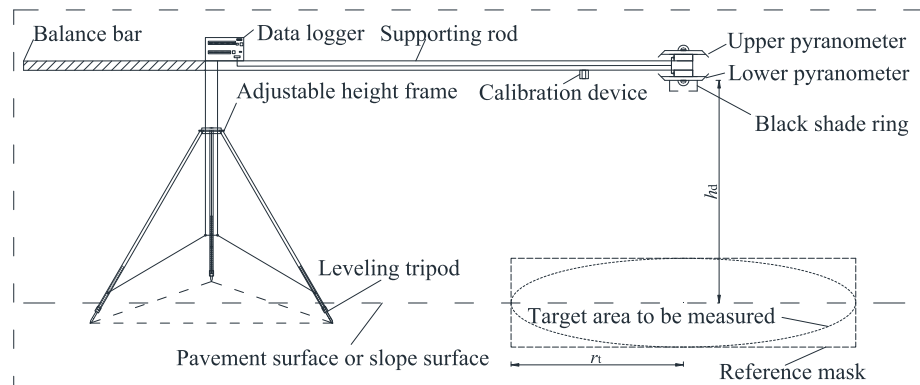


Fig. 3. Schematic of the measurement system.

$$R_m = I_m \rho_m F_{d-usd} + k I_m \rho_m F_{d-sd} + I_m \rho_m F_{w-m} \rho_w F_{d-w} + I_m \rho_{sur} F_{w-sur} \rho_w F_{d-w} + R_e \quad (4)$$

where I and R are the readings of the upper and lower pyranometers, W/m^2 ; k is the proportion of diffuse radiation to global horizontal irradiance; the subscripts of “s”, “d”, “usd”, “sd”, “w”, “sur”, “m”, “e”, “ai”, “ao”, “wi”, “wo” respectively stand for the slope surface, the detector of lower pyranometer, the un-shaded area of the measurement area, the shaded area of the measurement area, the inner wall of the shade ring, the surrounding environment, the reference mask, the source of other measurement errors, the inner side of the opaque annulus, the outer side of the opaque annulus, the inner side of the nominal disk, and the outer side of the nominal disk (Fig. 5). Here, the surface albedos for the sunlit and shadowed areas are considered as the same value due to the minor difference.

Based on the calculation principles (Howell, 1982), the related view factors can be calculated as

$$F_{d-s} = F_{d-a} = \frac{1}{2} \left\{ 1 + \left(\frac{h_w}{r_d} \right)^2 + \left(\frac{r_a}{r_d} \right)^2 - \left\{ \left[1 + \left(\frac{h_w}{r_d} \right)^2 + \left(\frac{r_a}{r_d} \right)^2 \right]^2 - 4 \left(\frac{r_a}{r_d} \right)^2 \right\}^{\frac{1}{2}} \right\} \quad (5)$$

$$F_{d-w} = \frac{1}{2} \left\{ 1 - \left(\frac{h_w}{r_d} \right)^2 - \left(\frac{r_w}{r_d} \right)^2 + \left\{ \left[1 + \left(\frac{h_w}{r_d} \right)^2 + \left(\frac{r_w}{r_d} \right)^2 \right]^2 - 4 \left(\frac{r_w}{r_d} \right)^2 \right\}^{\frac{1}{2}} \right\} \quad (6)$$

$$F_{sur-w} = F_{a-w} = \frac{1}{2} \left\{ 1 - \left(\frac{h_w}{r_a} \right)^2 - \left(\frac{r_w}{r_a} \right)^2 + \left\{ \left[1 + \left(\frac{h_w}{r_a} \right)^2 + \left(\frac{r_w}{r_a} \right)^2 \right]^2 - 4 \left(\frac{r_w}{r_a} \right)^2 \right\}^{\frac{1}{2}} \right\} \quad (7)$$

According to the reciprocity relation, the other related view factors can be derived as

$$F_{w-sur} = F_{sur-w} \frac{r_a^2}{2r_w h_w} \quad (8)$$

The parameters r_d , r_w , r_a , and h_w are set as 11 mm, 50 mm, 25 mm, and 35.2 mm, respectively, in this study. Based on these parameters, we can yield that $F_{d-s} = 0.321$, $F_{d-w} = 0.339$, and $F_{w-sur} = 0.066$. The other measurement errors R_e can be obtained

$$R_e = [I_s \rho_s F_{ao-s} + I_s \rho_{sur} F_{ao-sur}] \rho_{ao} F_{s-ao} \rho_s F_{d-s} + I_s \rho_{sur} F_{w-sur} \rho_w (F_{ai-w} \rho_{ai} F_{d-ai} + F_{w-w} \rho_w F_{d-w}) \quad (9)$$

The interior wall of the shade ring is painted with a low reflective coating ($\rho_w = \rho_{ai} = 0.05$) to minimize the measurement errors. The albedo of this low reflective coating is calculated by Eq. (1) (Fig. 2). In consideration of the extreme situations, the related parameters are set as $I_s = 1000 \text{ W/m}^2$ and $\rho_s = \rho_{sur} = \rho_{ao} = 1.0$. The latter three items in Eq. (3) and Eq. (4) are less than 3.0 W/m^2 in the most disadvantaged condition, which can be ignored (Wang et al., 2019). For the convenience of calculation, the view factors of the detector to the measured area for both slope surface and reference mask are assumed as the same value due to the small difference. In other words, the parameters, F_{d-usd} and F_{d-

sd , are set as the values for the slope surface and reference mask surface under test.

Substituting Eq. (3) into Eq. (4), the slope surface albedo can be determined as (Wang et al., 2019)

$$\rho_s = \rho_m I_m R_s / I_s R_m \quad (10)$$

It's worth noting that the incident radiation received by the upper pyranometer consists of the solar radiation and the radiation reflected by the surrounding natural ground surface. This is one of the biggest differences between the previous measurement methods and the proposed method. In this condition, the incident radiation received by the upper pyranometer can be described as

$$I_s = I_{s-\text{solar}} + I_{s-\text{ground}}, \quad I_m = I_{m-\text{solar}} + I_{m-\text{ground}} \quad (11)$$

where $I_{s-\text{solar}}$ and $I_{m-\text{solar}}$ are the incident solar radiation received by the upper pyranometers, W/m^2 ; $I_{s-\text{ground}}$ and $I_{m-\text{ground}}$ are the reflected ground radiation received by the upper pyranometers, W/m^2 . The

values, I_s and I_m , are determined by the solar position, slope angle, embankment orientation, slope position, surface roughness, and nearby ground surface albedo.

3. Experiments

To study the influence of different methods on the albedo measurement results of embankment surfaces. We carried out the following experiments.

3.1. Solar albedo of pavement surface

The experimental site is chosen at the Beiluhe area of the Qinghai-Tibet Plateau (E 92.92° and N 34.82°), China. It adjoins the Qinghai-Tibet Highway and the Qinghai-Tibet Railway. Thus, the experiment results are representative. The experiment was carried out on an embankment in permafrost regions of the Qinghai-Tibetan Plateau (Fig. 6). The average road width exceeds 5.0 m and the slope length is about 8–9 m, which meets the experiment requirements. Both pavement and slope surfaces consist of the gravel soils. In this study, two methods were used to measure the pavement surface albedo of the experiment embankment (Fig. 6). Detailed information is listed in Table 1. The type of pyranometer is CMP 11. Its measurement ranges are from 310 to 2800 nm, and the measurement error is less than 7 W/m^2 (within 200

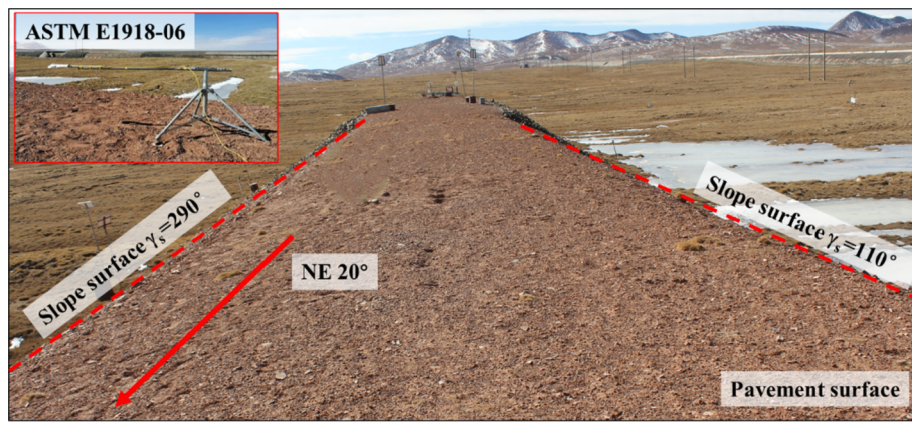


Fig. 6. The experiment embankment in permafrost regions.

Table 1
Albedo measurement methods and relevant equipments.

Number	Method	Main equipment	Target area to be measured (m ²)
N1	ASTM E1918-06	Two pyranometers	≥ 4
N2	Proposed method	Two pyranometers One black shade ring One reference mask	≥ 1

W/m²). The spectral reflectance of the reference mask is shown in Fig. 2.

For the method of ASTM E1918-06, the measurement equipment is leveled and centered over the pavement surface such that the lower pyranometer is set at a 0.5 m height. In this case, the effective surface under test is always on the pavement surface. The target area is about 4 m². According to Akbari et al. (Akbari et al., 2008), the albedo of pavement surface can be acquired using the following formula:

$$\rho_{E1918} = I_{E1918}/R_{E1918} \quad (12)$$

where I_{E1918} and R_{E1918} are the readings of the upper and lower pyranometers based on the ASTM E1918-06.

To validate the proposed method, we measure the pavement surface albedo same as the method of ASTM E1918-06. The detailed measurement principle is shown in Fig. 3. The procedure for measuring the pavement surface includes:

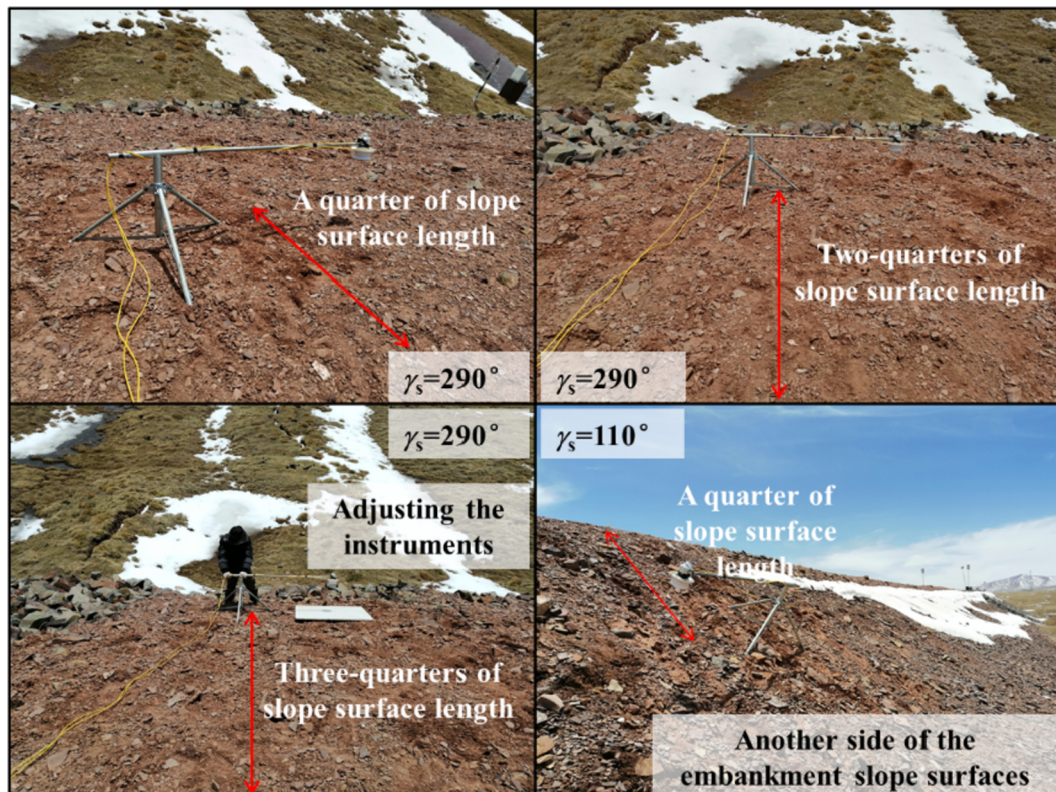


Fig. 7. In-situ albedo measurements at different locations of the embankment slopes.

- (1) Installing the upper and lower pyranometers on the supporting rod and making sure the parallelism of two sensors;
- (2) Adjusting the pyranometers at 0.5-m height above the measured slope surface and placing the supporting rods towards the sun position to minimize shadowed areas;
- (3) Covering the measurement area with a white reference mask;
- (4) Reading the incident radiation I (I_p and I_m) and the reflected radiation R (R_p and R_m) simultaneously for both pavement surface and reference mask surface;
- (5) Calculating the surface albedos of different types based on Eq. (13), if the maximum difference between I_p and I_m doesn't exceed 20.0 W/m²; otherwise, repeating steps (3)-(5);
- (6) Monitoring the solar albedo until the solar or weather condition is not suitable to continue the experiment.

Using the measurement procedure above, we can obtain the pavement albedo by the following formula:

$$\rho_p = \rho_m I_m R_p / I_s R_m \quad (13)$$

3.2. Solar albedo of slope surface

To verify the proposed albedo measurement method of embankment slope surface, the experimental embankment was chosen the same as Fig. 6. It's worth noting that the pavement surface and slope surface of the experimental site are covered by the same material, namely gravel soil. Due to a lack of systematic albedo measurement method of embankment slope surface, the verification process is different from the previous methods. In this study, we verify the proposed measurement method in two steps. In the first step, we verify the proposed method by comparing the measurement results of pavement surface albedo with the ASTM E1918-06 method. In the second step, we compare the measured pavement albedo and slope surface albedo based on the proposed method (Fig. 7). If the results are the same or within the allowed error range, the proposed method can be verified. The procedure for measuring the embankment slope surface is similar to the procedure for pavement surface. Different procedure is listed as follows:

- (1) Adjusting the pyranometers and measuring instruments parallel to the slope surface by the calibration device (Figs. 3–4);
- (2) Reading the incident radiation I (I_s and I_m) and the reflected radiation R (R_s and R_m) simultaneously for both slope surface and reference mask surface;

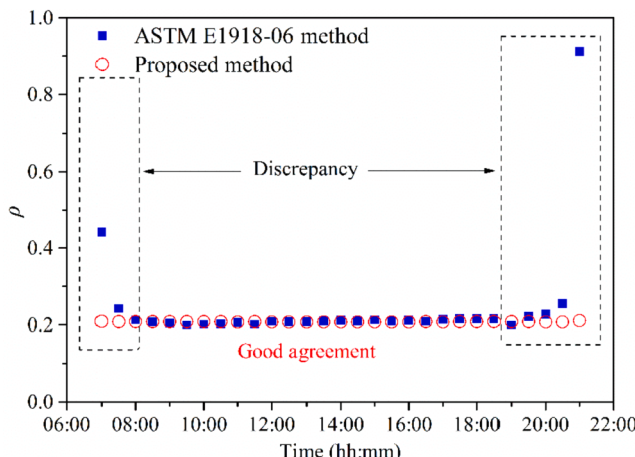


Fig. 8. Albedo measurement results of pavement surface by using the ASTM E1918-06 method and the proposed method.

- (3) Calculating the surface albedos of different types based on Eq. (14), if the maximum difference between I_s and I_m doesn't exceed 20.0 W/m²; otherwise, repeating above steps;
- (4) Monitoring the solar albedo until the solar or weather condition is not suitable to continue the experiment.
- (5) If the slope length is longer than 2.0 m, the albedo values should be estimated at certain intervals. Meanwhile, the measured mean value is regarded as the slope surface albedo. If the embankment slope consists of different engineering materials (e.g. soil and crushed rock), the albedo values should be measured separately.

The slope surface albedo can be determined by Eq. (14):

$$\rho_s = \rho_m I_m R_s / I_s R_m \quad (14)$$

4. Results and discussions

4.1. Measured albedo of pavement surface

ASTM E1918-06 method is an accepted method of albedo measurement. The albedo values are estimated by the ASTM E1918-06 method and the proposed method based on the Eqs. (12)–(13), which are shown in Fig. 8. The results indicate that the measured albedo values of pavement surface are very close from 8:00 am to 6:00 pm. The maximum difference is less than 0.008. The relative error is less than 5%. Within this time period, the measurements are reasonable. The deviations between these two methods mainly result from the different sizes of the measurement area. Of course, the deviations may also come from the errors of the reference mask surface, of the black shade ring, of the operating and measuring procedures. Although there are some minor deviations, the measured albedo values of the proposed method agree well with the ASTM E1918-06 method.

However, Fig. 8 also shows that the albedo values estimated by the two methods are much more different from each other when the measured time is before 8:00 am and after 6:00 pm. The albedo values measured by the ASTM E1918-06 method deviate from the reasonable values at these times. It is because that part of the solar incident light could be received by the lower pyranometer detector when the solar altitude is small. The albedo values estimated by Eq. (12) are not applicable anymore. Whereas, the proposed method is still valid in this case due to the special measuring equipment. The black shade ring can not only isolate the radiations that are not reflected by the slope surface, but also the solar incident radiations.

There are a few things we can learn from the experiment results. Firstly, the proposed method can reliably measure the albedo of the pavement surface and the related engineering surfaces. Secondly, this

Table 2

Measured albedo values of the pavement surface and the slope surfaces based on the proposed method.

Time	Pavement surface Center	Slope surface $\gamma_s = 290^\circ$			Slope surface $\gamma_s = 110^\circ$		
		1/4	2/4	3/4	1/4	2/4	3/4
7:00	0.209	0.214	0.212	0.211	0.214	0.208	0.207
8:00	0.208	0.198	0.191	0.192	0.211	0.196	0.199
9:00	0.208	0.197	0.190	0.191	0.198	0.191	0.187
10:00	0.208	0.197	0.185	0.185	0.195	0.188	0.189
11:00	0.208	0.186	0.183	0.181	0.195	0.182	0.185
12:00	0.208	0.187	0.190	0.188	0.192	0.183	0.183
13:00	0.208	0.189	0.189	0.190	0.186	0.183	0.183
14:00	0.208	0.194	0.192	0.192	0.184	0.185	0.184
15:00	0.208	0.199	0.191	0.192	0.184	0.180	0.178
16:00	0.208	0.201	0.192	0.194	0.185	0.185	0.187
17:00	0.208	0.207	0.205	0.200	0.194	0.188	0.188
18:00	0.208	0.218	0.210	0.203	0.197	0.206	0.194
Mean values		0.199	0.194	0.193	0.195	0.189	0.189
Mean difference values		0.009	0.014	0.015	0.013	0.019	0.019

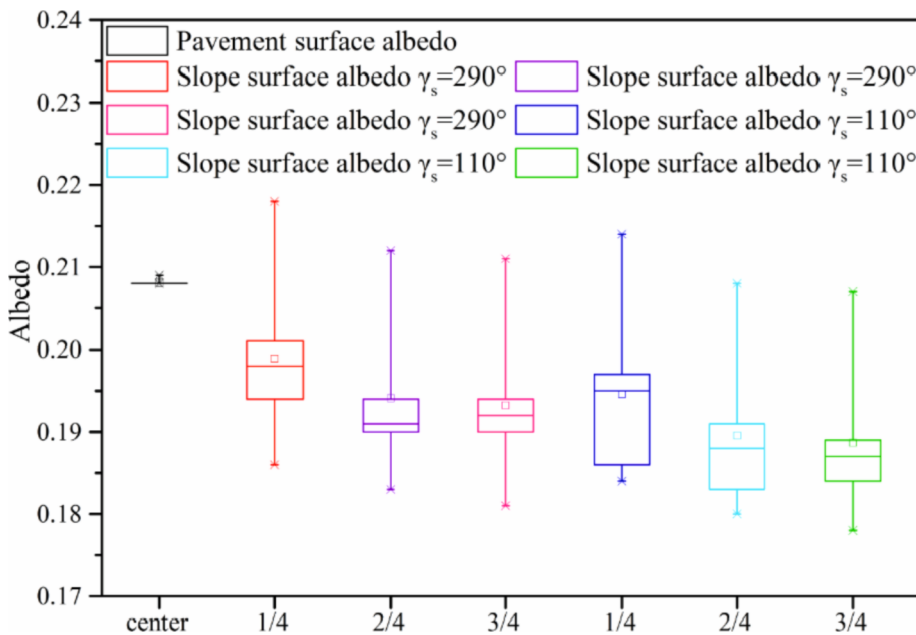


Fig. 9. The box diagram of albedo measurement results for pavement and slope surfaces at different positions.

method is less affected by the surrounding environmental factors, especially the incoming sunlight. Finally, the proposed method can reduce the post-processing of the test data. Because we no longer need to manually remove unreasonable data collected by the automatic monitoring devices.

4.2. Measured albedo of slope surface

Table 2 shows the measured albedo values of the experimental embankment surfaces, including pavement surface and two embankment slope surfaces (Fig. 7). As the surfaces are made up of the same filling material (gravel soil), the surface albedo values should be very close. The results display that the measured albedo values of the pavement surface and slope surfaces differ little within a day. The maximum differences and the minimum differences between pavement surface and slope surface are 0.019 and 0.009, respectively. The minimum relative error does not exceed 7%. It indicates that the proposed measurement method could also apply to the embankment slope surfaces according to our verification process. As we can see from the box diagram in Fig. 9, there is some discreteness in the measured albedo values of the slope surface. But the dispersion degree is relatively low. Comparing with pavement surface albedo, all the mean albedo values of slope surfaces are lower, while the maximum values are larger. The reasons for these phenomena can be attributed to the following aspects. Although the filling material of the embankment is the same for both pavement and slope surfaces, there are still some differences. Some crushed rocks with lower albedo appear more frequently on the slope surface, which leads

to lower mean albedo values of slope surfaces. Meanwhile, there are more crushed rocks on the slope surface near slope toe or facing to the west ($\gamma_s = 110^\circ$). These conditions are in good agreement with the experimental results. Furthermore, the measured results are also affected by the errors of measurement processes, the solar position, the slope conditions, the snow cover, aeolian sand, and the multiple reflection effect between slope surface and natural ground surface. Relevant studies (Qin et al., 2016a; Qin et al., 2017) show that multiple reflection effects would increase the incident radiation on slope surface, especially for the condition of high ground surface albedo. It is still not certain whether which factor dominates in this case. But we can make sure that the multiple reflection effect is one of the main causes of data dispersion. Despite these minor deviations, the proposed method still shows strong applicability. Of course, we will improve the experiment and measurement methods in the follow-up studies. Based on our experimental experience, we offer two recommendations for slope albedo measurement. One is to choose a position as close to the top of the slope as possible for the measurement. Another is to try to choose a time of day when the sun is directly over the slope to take the measurement.

4.3. Comparison of the improved method and the traditional methods in determining slope surface albedo

We summary some possible conditions if traditional measurement methods would be used to determine the solar albedo of engineering slope surface (ASTM-E1918-06, 2006; Sailor et al., 2006; Levinson et al., 2010a, b; Qin et al., 2016a; Mei et al., 2017; Levinson et al., 2020). The

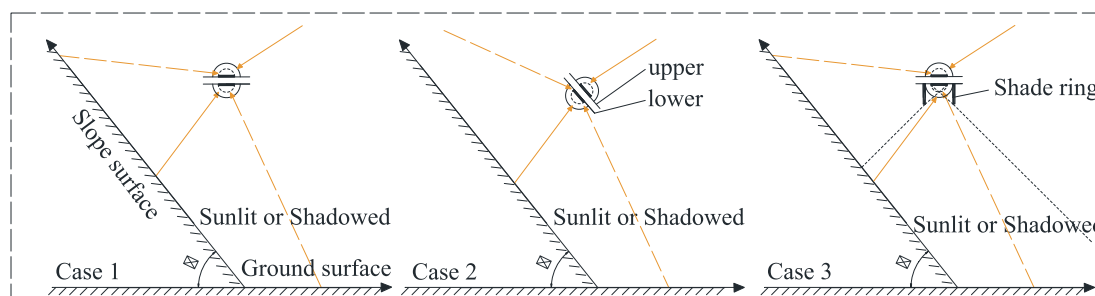


Fig. 10. Traditional measurement methods in determining solar albedo of engineering slope surface.

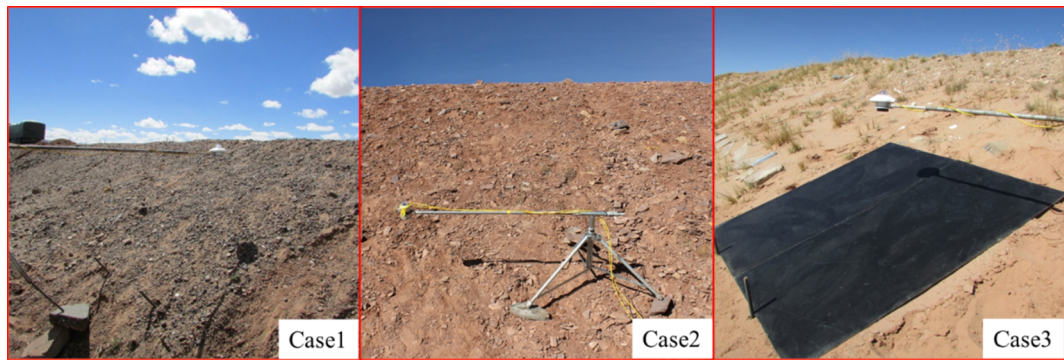


Fig. 11. In-situ experiment pictures of the traditional measurement methods.

Table 3

The main measurement errors for traditional methods.

Conditions	Source of measurement errors			
	Slope surface	Surrounding environment	Solar radiation	Shadowed area
Case 1	✓	✓	✗	✓
Case 2	✓	✓	✓	✗
Case 3	✓	✓	✗	✓

measurement diagram and in-situ experiment pictures are shown in Figs. 10–11, respectively. We discuss three main scenarios (Case 1 to Case 3) as shown in the diagrams. The main sources of measurement errors are analyzed in Table 3. Instrument errors and measurement errors are not listed in the table as secondary errors.

As for case 1 and case 3, the pyranometers are placed horizontally. In these cases, the upper pyranometer could always receive the total incident radiations while the lower pyranometer couldn't receive the reflected part of beam radiation when the slope surface is shadowed. The

undesired radiations received by the pyranometers are plotted as the yellow dotted lines in Fig. 10. These radiation values will seriously affect the correctness of the albedo measurement results. The upper pyranometer may receive the undesired radiations that are reflected by the slope surface, while the lower pyranometer may receive the undesired radiations that are reflected by the surrounding ground surface. Besides, these two cases ignore the influence of multiple reflection effects between slope and ground surface, which also increases the measurement errors. Although the pyranometers are set parallel to slope surface for case 2, it is always difficult to determine the view factor between the lower pyranometer and slope surface. The undesired radiations mainly come from the solar incident radiation and the radiation reflected by the surrounding ground surface. When the slope length is short, the measured albedo values will be grossly overestimated.

The proposed method shown in Fig. 4 can effectively solve these problems and diminish these errors whether the slope and ground surfaces are sunlit or shadowed. Measurement results are not compared between the traditional method and the proposed method. It is because that the albedo measurement results of the traditional method are

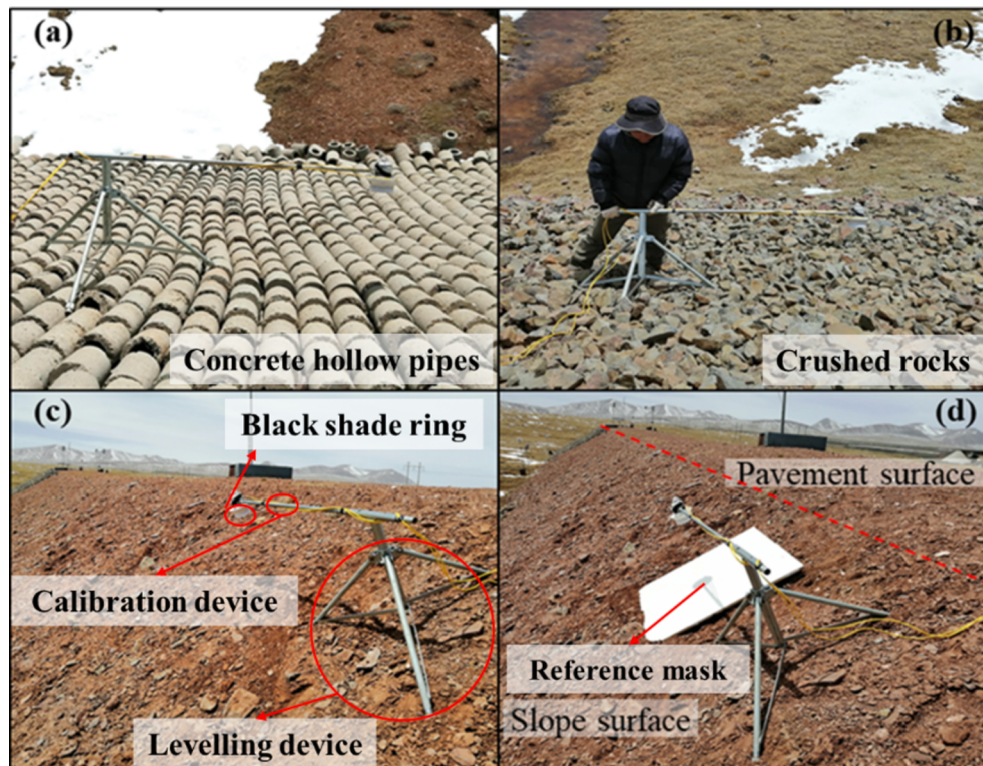


Fig. 12. Albedo measurements of slope surfaces with different materials.

Table 4

Albedo measurements of the slope surfaces covered by crushed rocks and concrete hollow pipes.

Surface cover	Slope surface $\gamma_s = 290^\circ$		Slope surface $\gamma_s = 110^\circ$	
	Range	Mean values	Range	Mean values
gravel soil 2/4	0.183–0.212	0.194	0.182–0.208	0.189
concrete hollow pipes 2/4	0.273–0.300	0.282	0.275–0.302	0.283
crushed rocks 2/4	0.155–0.182	0.166	0.157–0.183	0.168

influenced by many factors, such as slope length, slope albedo, slope azimuth, solar azimuth, surrounding ground albedo, etc. These factors contribute to the uncertainty and variability of the measurement results. Even for the same slope, the measurement results vary greatly within a day. Comparing with the proposed method, the measurement results are not regular and representative, either higher or lower. It should be noted that these traditional measurement methods are still suitable for slanting roofs in some cases (Levinson et al., 2020). Because the measurement processes and influencing factors are not complicated in this situation. The biggest difference is the presence of the natural ground around the embankment.

4.4. Albedo measurements of slope surfaces covered by different materials

To ensure the stability of permafrost roadbeds, researchers have developed a variety of roadbed structures, such as crushed rock roadbed, concrete hollow pipes roadbed, sunshade roadbed, etc. These structures not only change the characteristics of the embankment slope surface, but also change the heat exchange process. Hence, it is worth studying the albedo of the embankment slope surface with different kinds of materials. Two typical slope surfaces were selected for measurement and verification, namely crushed-rock slope, and hollow pipe slope (Fig. 12).

Table 4 shows that the measured surface albedo values agree well for different slope directions. It further verifies the feasibility of the proposed measurement method. The dispersion degrees of crushed rock and concrete hollow pipe surfaces are lower than that of gravel soil surfaces due to relatively uniform material composition. However, there is a small range of dispersion. The crushed rock and concrete hollow pipe surfaces are rougher and have more small holes. It would increase the multiple reflections between hole walls and change the transfer process of solar radiation between the slope and surrounding ground surface. This is one of the main reasons for the data dispersion. In addition, flat reference plates are distinguished from the rough and irregular slope surfaces. In the further research, we will further improve the equipment to solve above problems.

Based on the proposed measured method, we measured the albedo of the embankment surfaces in permafrost regions along the Highway G109 (K2800-K3400). We surveyed a 600 km stretch of the Highway G109 including about 550 km roads in permafrost zones. Fig. 13 and Table 5 show the measurement results. About 7.27% of these embankments are labeled by “no slope”. In these sections, the roadbed and base course are built beneath the natural ground surface, or the fill height of the embankment is low. As for the asphalt pavements, the surface albedo values are relatively low. Although the albedo values among 0.1 ~ 0.15 account for 90.68% of the total values, the albedo mean value is only 0.10. A low reflective pavement surface would greatly increase the solar radiation absorption, which reduces the thermal stability of permafrost embankment. Although the surface albedo of the asphalt pavement increases with age, the increasing degree is small. Meanwhile, there are more disease problems on asphalt surfaces in permafrost, such as cracks, potholes, patches. These diseases need to be repaired by new asphalt materials with low reflectivity. It would further increase heat absorption and exacerbate the damage.

To investigate the heat reflection properties of the embankment slope surfaces, we carried out a series of experiments based on the

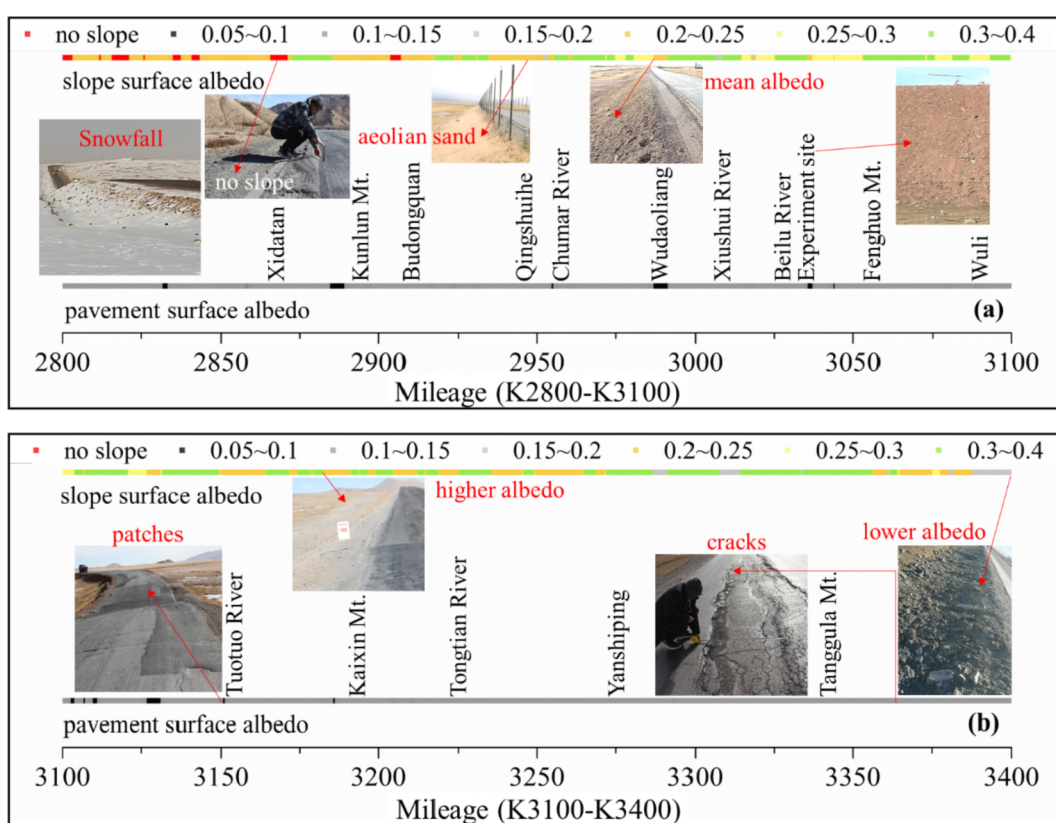
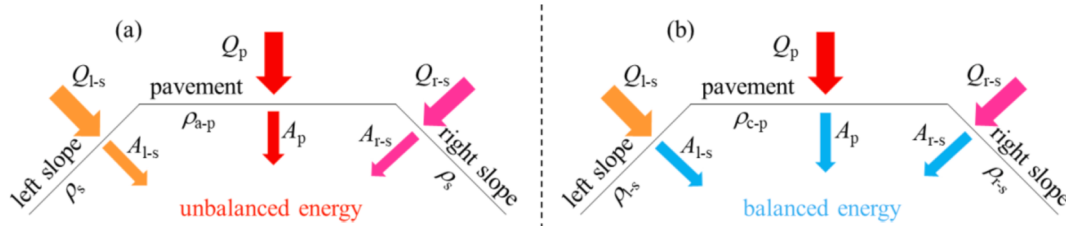


Fig. 13. Albedo measurements of the pavement and slope surfaces along the Highway G109.

Table 5

Albedo measurement results of pavement and slope surfaces along the Highway G109.

Surface type	Albedo measurement values						mean
	0.05 ~ 0.1	0.1 ~ 0.15	0.15 ~ 0.2	0.2 ~ 0.25	0.25 ~ 0.3	0.3 ~ 0.4	
pavement surface	9.32%	90.68%	–	–	–	–	0.10
slope surface	–	–	10.19%	40.86%	12.39%	36.54%	0.24

**Fig. 14.** Schematic diagram of albedo adjustment scheme.

proposed method. The surface albedo values among 0.15 ~ 0.2, 0.2 ~ 0.25, 0.25 ~ 0.3, 0.3 ~ 0.4 are 10.19%, 40.86%, 12.39% and 36.54%, respectively. The slope surface with higher albedo is influenced by the aeolian sand, which albedo is generally greater than 0.30. Only 1.99% of albedo values are greater than 0.35 when desertification is serious. Although the aeolian sand can increase slope albedo to a small extent, we are still not sure whether it will improve the thermal stability of the embankment. It might even exacerbate uneven settlement of the embankment or reduce the convective heat transfer performance of crushed-rock embankment. Similar to the asphalt pavement, the mean slope albedo is also low, only 0.24. The survey results indicate that the permafrost embankment consistently absorbs large amounts of solar radiation. This largely affects the thermal stability of the embankment, especially in permafrost regions with high temperatures and high ice content. There is also a relationship between the embankment diseases and the low reflectivity properties of the embankment surface, but the relevance needs further study.

Based on the above research results, we consider that a method of regulating embankment surface albedo can be used to improve the stability of the permafrost embankment and reduce embankment distress (Fig. 14). It can be achieved by covering the surface with high reflectivity materials, such as heat-reflective coating materials and high reflective engineering materials. In the case of considering only the influence of radiation on the thermal boundary condition of embankment surfaces, the albedo control scheme can be preliminarily determined by the following formula:

$$Q_p(1 - \rho_{c-p}) = Q_{l-s}(1 - \rho_{l-s}) = Q_{r-s}(1 - \rho_{r-s}) \quad (15)$$

where Q is the annual mean total incident radiation intensity; A is the energy entering the interior of the embankment; the subscripts of “a-p”, “c-p”, “s”, “l-s”, and “r-s” stand for the asphalt pavement surface, the pavement surface with high albedo value, the original slope surface, the left slope surface with high albedo value, and the right slope surface with high albedo value, respectively. The parameter Q can be

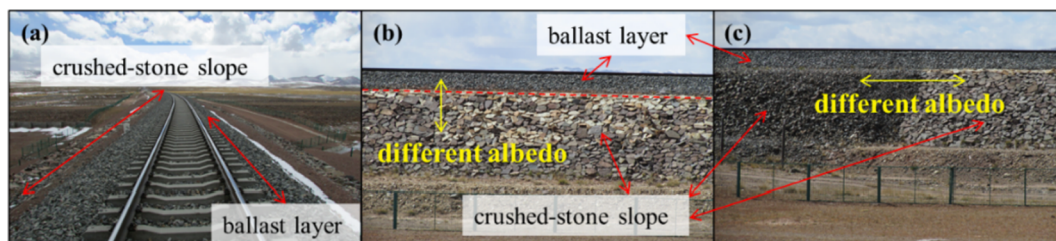
determined by the in-situ monitoring value or the empirical formula value. It is worth noting that Eq. (15) only displays the preliminary proposal. The thermal boundary conditions of embankment surfaces are also affected by the climatic environment, the material attribute, the sunny-shady slope, and other factors. According to the actual situation, this scheme needs to be further adjusted to achieve accurate temperature control of permafrost embankment.

In conclusion, the proposed method is suitable for the albedo measurement of highway embankment surfaces. Meanwhile, this approach is also applicable to other linear projects or embankment slopes in permafrost regions. Fig. 15 shows the typical embankment surfaces of the Qinghai-Tibet Railway. Fig. 16 displays the typical embankment structures and the characteristics of crushed-stone slopes. Large differences in the albedo values of the embankment surfaces are due to the different material types, material sizes, and structure positions. These differences could lead to uneven distribution of temperature fields in the embankment. Hence, it is necessary to carry out researches on the albedo measurement methods of embankment slope surfaces.

4.5. Comparison of the measurement results and the remote sensing data

The embankment surface albedo is not only affected by human engineering activities, but also influenced by the natural environmental factors, including the drifting snow, snowfall, aeolian sand, solar azimuth, etc. These factors would permanently or periodically change the original albedo of permafrost embankment surfaces. It has a great influence on the energy balance of the embankment, so these factors need to be evaluated.

This experiment measured the original surface albedo along the Highway G109 (K2800 + 000-K3400 + 000). Meanwhile, we measured the albedo values of several typical aeolian sands along the route, which range from 0.32 to 0.38. The mean value is about 0.35. In comparison, the snow albedo is less variable, which is about 0.80–0.90. But the albedo of embankment surface covered by snow is influenced by the

**Fig. 15.** Typical embankment surfaces of the Qinghai-Tibet Railway.

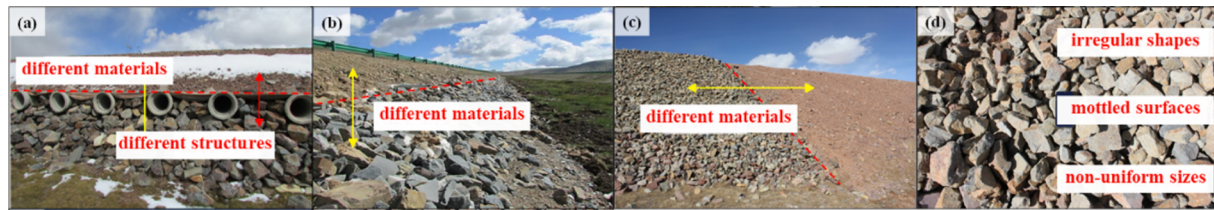


Fig. 16. Typical embankment structures and characteristics of the crushed-stone slopes in the Qinghai-Tibet Plateau.

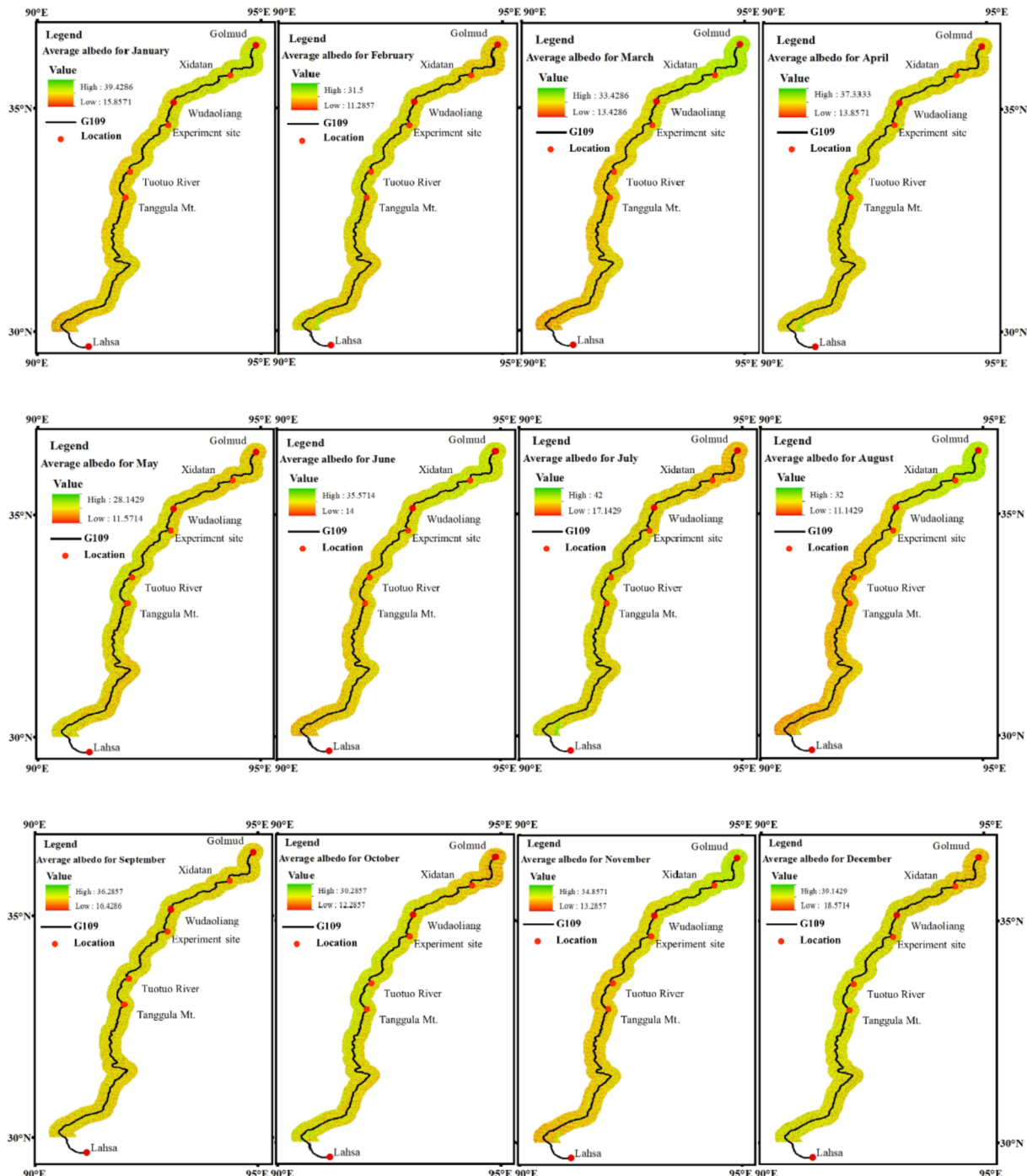


Fig. 17. Monthly average albedos of the natural ground surfaces along the Highway G109.

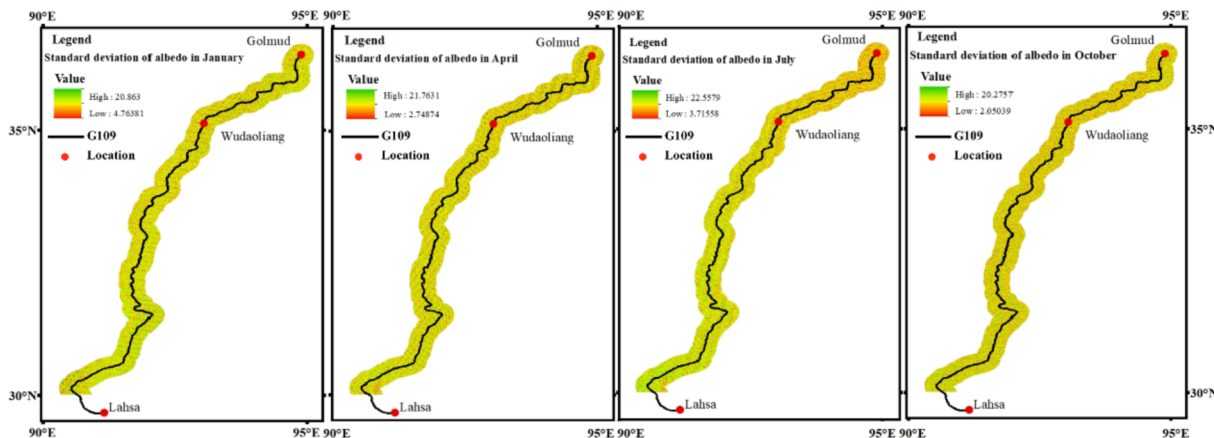


Fig. 18. The standard deviation of the albedo values in a month along the Highway G109.

coverage degree and snowfall dates (Fig. 13). This also increase the randomness and the uncertainty of the albedo in embankment surface. Therefore, we used the remote sensing data to analyze the variation of natural ground surfaces in monthly mean albedo over the course of a year (Fig. 17). The data is available from EARTHDATA-MOD09GQ (MODIS/Terra Surface Reflectance Daily L2G Global 250 m SIN Grid V006). The resolution of the MODIS data is 250 m. As shown in Fig. 17, there are variations among the monthly average albedo. These differences are mainly due to the changes in the condition of the underlying surface, including vegetation coverage, snow depth, aeolian sand coverage, etc. In the surveyed area, the mean albedo does not change significantly. But the remote data are higher than the measurement values. It is because the albedo values of embankment materials are generally lower than the natural ground surfaces. To further explore the dispersion of the data, we made standard deviations for the monthly albedo values (Fig. 18). Because of space constraints, we select four months to analyze the dispersion. The results indicate that standard deviations of the albedo values are not very large in a month. Although snowfall greatly increases the surface albedo, the snow cover does not last long. It also explains why the differences among the monthly mean reflectance are not very prominent.

Since the high-precision remote sensing data is more difficult to obtain, the measurement method proposed in this paper is more applicable in solving the problem of the practical engineering designs. However, with the application of remote sensing data analysis, we can study the changes of embankment surface albedo under the influence of environmental factors in a particular study area. By comparison, we can further understand the albedo changes in the natural surface after construction of the embankment. It would help us to adjust the albedo regulation scheme of the embankment surfaces based on Eq. (15).

The next relevant researches will focus on two aspects. On the one hand, we would continue to investigate techniques for observing the embankment surface albedo in permafrost regions, and further extend the method to measure the albedos of engineering surfaces in other permafrost regions. For example, using the UAV (unmanned aerial vehicle) observation technology to improve the resolution and study the albedo changes. On the other hand, we will further develop the albedo regulation scheme of the embankment surfaces to achieve the precise control of the embankment temperature field.

5. Conclusions

In this research, we study the characteristics of the solar albedo of embankment surfaces in permafrost regions. To improve the albedo measurement accuracy, a dual pyranometer-based measurement method was proposed for both pavement and slope surfaces. The proposed measurement method is proven to be effective by comparing the

experimental results with the ASTM E1918-06 method. Meanwhile, we measure the solar albedo of several typical slope surfaces for both sides, which exhibits good agreements. These findings prove that this method is suitable for both pavement and slope surfaces. The shortcomings and limitations of traditional measurement methods in determining slope surface albedo are also discussed. Based on the proposed method, we measure the solar albedos of the pavement and slope surfaces of the Qinghai-Tibet Highway in permafrost regions. The results indicate that the albedo values of these embankment surfaces are low, which would exacerbate the embankment diseases and the sunny-shady slope effect. Therefore, a preliminary solution is suggested to solve the problems of the low surface albedos and the uneven solar radiation absorption of embankment surfaces. Finally, we use the remote sensing data to analyze the surface albedo values along the Qinghai-Tibet Highway in permafrost regions. The results show that the resolution is still not enough to analyze the solar albedo characteristics of pavement and embankment slope surfaces. But the remote sensing data display the spatial and temporal variations of the underlying surface albedos. It is beneficial to develop the albedo measurement method and energy balance theory of permafrost embankment. Further research will focus on the developments of the albedo measurement method and albedo regulation scheme for the embankment surfaces in permafrost regions.

Declaration of Competing Interest

The authors declare that they have no known competing financial interests or personal relationships that could have appeared to influence the work reported in this paper.

Acknowledgments

This work was supported by the National Natural Science Foundation of China (Grant Nos. 41825015, 42101140), the CAS “Light of West China” Program for the Belt and Road Research Teams (Granted to Dr. Mingyi Zhang), the National Natural Science Foundation of China (Grant No. 42011530087), the Natural Science Foundation of Inner Mongolia Autonomous Region (Grant No. 2021BS05004), the Program of the State Key Laboratory of Frozen Soil Engineering (Grant No. SKLFSE202103), and the Special Research Assistant Program of the Chinese Academy of Sciences (Granted to Dr. Ruiqiang Bai).

References

- Akbari, H., Levinson, R., Stern, S., 2008. Procedure for measuring the solar reflectance of flat or curved roofing assemblies. *Sol. Energy* 82 (7), 648–655.
- ASTM-C1549-09, 2002. Standard test method for determination of solar reflectance near ambient temperature using a portable solar reflectometer, ASTM International, West Conshohocken, PA.

- ASTM-E903-12, 2012. Standard test method for solar absorptance, reflectance, and transmittance of materials using integrating spheres, ASTM International, West Conshohocken, PA.
- ASTM-E1918-06, 2006. Standard Practice for Calculating Solar Reflectance Index of Horizontal and Low-Sloped Opaque Surfaces, ASTM International, West Conshohocken, PA.
- Cai, D., Yan, H., Yao, J., Cui, Y., Chen, F., 2016. Engineering Test Research of XPS Insulation Structure Applied in High Speed Railway of Seasonal Frozen Soil Roadbed. *Procedia Eng.* 143, 1519–1526.
- Cheng, G., Sun, Z., Niu, F., 2008. Application of the roadbed cooling approach in Qinghai-Tibet railway engineering. *Cold Reg. Sci. Technol.* 53 (3), 241–258.
- Chou, Y., Sheng, Y., Wei, Z., Ma, W., 2008. Calculation of temperature differences between the sunny slopes and the shady slopes along railways in permafrost regions on Qinghai-Tibet Plateau. *Cold Reg. Sci. Technol.* 53 (3), 346–354.
- Chou, Y., Sheng, Y., Zhu, Y., 2012. Study on the relationship between the shallow ground temperature of embankment and solar radiation in permafrost regions on Qinghai-Tibet Plateau. *Cold Reg. Sci. Technol.* 78, 122–130.
- Doré, G., Niu, F., Brooks, H., 2016. Adaptation methods for transportation infrastructure built on degrading permafrost. *Permafrost Periglac. Process.* 27 (4), 352–364.
- Fernández-García, A., Sutter, F., Martínez-Arcos, L., Sansom, C., Wolfertstetter, F., Delord, C., 2017. Equipment and methods for measuring reflectance of concentrating solar reflector materials. *Sol. Energy Mater. Sol. Cells* 167, 28–52.
- Howell, J.R., 1982. A catalog of radiation heat transfer configuration factors. McGraw-Hill, New York.
- Jin, H., Yu, Q., Wang, S., Liu, L., 2008. Changes in permafrost environments along the Qinghai-Tibet engineering corridor induced by anthropogenic activities and climate warming. *Cold Reg. Sci. Technol.* 53 (3), 317–333.
- Lai, Y., Guo, H., Dong, Y., 2009. Laboratory investigation on the cooling effect of the embankment with L-shaped thermosyphon and crushed-rock revetment in permafrost regions. *Cold Reg. Sci. Technol.* 58 (3), 143–150.
- Levinson, R., Akbari, H., Berdahl, P., 2010a. Measuring solar reflectance-Part I: Defining a metric that accurately predicts solar heat gain. *Sol. Energy* 84 (9), 1717–1744.
- Levinson, R., Akbari, H., Berdahl, P., 2010b. Measuring solar reflectance-Part II: Review of practical methods. *Sol. Energy* 84 (9), 1745–1759.
- Levinson, R., Egolf, M., Chen, S., Berdahl, P., 2020. Experimental comparison of pyranometer, reflectometer, and spectrophotometer methods for the measurement of roofing product albedo. *Sol. Energy* 206, 826–847.
- Liu, H., Niu, F., Guan, H., 2017. An engineering evaluation index of thermal asymmetry in subgrade and its optimal design in cold regions. *Cold Reg. Sci. Technol.* 137, 1–6.
- Mei, G., Wu, B., Ma, S., Qin, Y., 2017. A simplified method for the solar reflectance of a finite surface in field. *Measurement* 110, 211–216.
- Pei, W., Zhang, M., Li, S., Lai, Y., Jin, L., 2017a. Enhancement of convective cooling of the porous crushed-rock layer in cold regions based on experimental investigations. *Int. Commun. Heat Mass Transfer* 87, 14–21.
- Pei, W., Zhang, M., Li, S., Lai, Y., Jin, L., Zhai, W., Yu, F., Lu, J., 2017b. Geotemperature control performance of two-phase closed thermosyphons in the shady and sunny slopes of an embankment in a permafrost region. *Appl. Therm. Eng.* 112, 986–998.
- Pei, W., Zhang, M., Wan, X., Lai, Y., Wang, C., 2021. Numerical optimization of the installing position for the L-shaped TPCT in a permafrost embankment based on the spatial heat control. *Sol. Energy* 224, 1406–1425.
- Qin, Y., He, H., 2017. A new simplified method for measuring the albedo of limited extent targets. *Sol. Energy* 157, 1047–1055.
- Qin, Y., Huang, H., Ying, J., Yang, T., 2017. Simulation of short-wave solar radiative transfer across a roadway embankment. *Int. J. Heat Mass Transf.* 108, 332–340.
- Qin, Y., Liang, J., Luo, Z., Tan, K., Zhu, Z., 2016a. Increasing the southern side-slope albedo remedies thermal asymmetry of cold-region roadway embankments. *Cold Reg. Sci. Technol.* 123, 115–120.
- Qin, Y., Luo, J., Chen, Z., Mei, G., Yan, L.-E., 2018. Measuring the albedo of limited-extent targets without the aid of known-albedo masks. *Sol. Energy* 171, 971–976.
- Qin, Y., Tan, K., Liang, J., 2016b. Theory and procedure for measuring the albedo of a roadway embankment. *Cold Reg. Sci. Technol.* 126, 30–35.
- Sailor, D.J., Resh, K., Segura, D., 2006. Field measurement of albedo for limited extent test surfaces. *Sol. Energy* 80 (5), 589–599.
- Tai, B., Liu, J., Yue, Z., Liu, J., Tian, Y., Wang, T., 2018. Effect of sunny-shady slopes and strike on thermal regime of subgrade along a high-speed railway in cold regions, China. *Eng. Geol.* 232, 182–191.
- Wang, J., Zhang, M., You, Z., Pei, W., Bai, R., 2019. A developed method to measure and calculate the solar albedo of discrete-particle layers. *Sol. Energy* 194, 671–681.
- Yu, Q., Pan, X., Cheng, G., He, N., 2008. An experimental study on the cooling mechanism of a shading board in permafrost engineering. *Cold Reg. Sci. Technol.* 53 (3), 298–304.
- Zhang, M., Pei, W., Li, S., Lu, J., Jin, L., 2017. Experimental and numerical analyses of the thermal-mechanical stability of an embankment with shady and sunny slopes in permafrost regions. *Appl. Therm. Eng.* 127, 1478–1487.
- Zhang, X., Yan, L.-E., Qin, Y., 2018. Regulating solar absorptance for remedying thermal asymmetry of a roadway embankment. *Int. J. Heat Mass Transf.* 121, 64–71.
- Zhang, Z., Yu, Q., Wang, J., Wang, X., Luo, X., 2021. Bidirectional convection mechanism and cooling performance of road embankment with a new duct-ventilated slope in permafrost regions. *Cold Reg. Sci. Technol.* 191, 103360.